Journal of
Vascular Diseases

MDPI

Article

Computed Tomography Imaging Features of Pulmonary Sequestration

Tingqian Yang [1,†], Zhaoyu Wang [2,†], Jun Qiang [3], Qinxiang Mao [4], Shufeng Kong [5], Zhonghua Sun [6,7,8,*] and Yu Li [1,*]

1 Department of Radiology, The Seventh Affiliated Hospital of Sun Yat-sen University, Shenzhen 518107, China; yang_ting_tian@126.com
2 Shanghai Xiawei Medical Examination Center, Shanghai 201100, China; wangzhaoyu8295@sina.com
3 Department of Imaging, The First Affiliated Hospital, College of Clinical Medicine, Henan University of Science and Technology, Luoyang 471003, China; 15838815301@163.com
4 Department of Radiology, Liuzhou People's Hospital, Liuzhou 530021, China; maoqx2014@sina.com
5 Department of Radiology, Jiangxi Cancer Hospital, Nanchang 330029, China; m15879049792@163.com
6 Discipline of Medical Radiation Science, Curtin Medical School, Curtin University, Perth, WA 6102, Australia
7 Curtin Health Innovation Research Institute (CHIRI), Curtin University, Perth, WA 6102, Australia
8 School of Medicine and Medical Advancement for Better Quality of Life Impact Lab, Taylor's University, Subang Jaya 47500, Malaysia
* Correspondence: z.sun@curtin.edu.au (Z.S.); liyu275@mail.sysu.edu.cn (Y.L.)
† These authors contributed equally to this work.

Abstract: Background: Pulmonary sequestration (PS), generally diagnosed using computed tomography pulmonary angiography (CTPA), is a rare congenital developmental malformation of the lung that is characterized by nonfunctional lung tissue, independent of the normal lung tissue. This paper summarizes the imaging features of the supplying arteries and draining vessels in patients with PS with an aim to assist in timely clinical diagnosis and operation guidance. Materials and Methods: A total of 55 patients with PS diagnosed using CTPA from multiple clinical centers were retrospectively analyzed. Data included demographic characteristics, imaging features, disease location, isolation type, and the features of supplying and draining vessels, as shown on CTPA images. Results: Of the 55 patients reviewed, 3 (5.45%) were children, 3 (5.45%) were adolescents, and 49 (89.09%) were adults; the mean age was 44 years. Fifty-four (98.18%) patients had intralobar sequestration and one (1.82%) had extralobar sequestration. PS was noted 3.5 times more frequently in the left lower lobe than in the right lower lobe. For the supplying arteries, 47 (85.45%) were derived from the descending thoracic aorta, 1 (1.82%) from the abdominal aorta, 7 (12.73%) from the celiac axis, and 1 (1.82%) from the bronchial artery. The draining vessels were the pulmonary veins in 49 patients (89.09%), the umbilical vein in 1 (1.82%), the venae intercostal in 1 (1.82%), the pulmonary arteries in 11 (20.00%), and the vessels were not shown on the images in 2 patients (3.64%). Conclusion: Clinical presentations of PS are non-specific and can be easily missed or misdiagnosed. However, CTPA can help to improve the diagnostic accuracy and identify the supplying arteries and draining vessels, which significantly contribute to surgical planning.

Keywords: pulmonary sequestration; computed tomography angiography; intralobar and extralobar sequestration; supplying artery; draining vessel

Citation: Yang, T.; Wang, Z.; Qiang, J.; Mao, Q.; Kong, S.; Sun, Z.; Li, Y. Computed Tomography Imaging Features of Pulmonary Sequestration. *J. Vasc. Dis.* **2023**, *2*, 367–380. https://doi.org/10.3390/jvd2040028

Academic Editors: Hsin-Fu Lee and Stefan Schob

Received: 11 June 2023
Revised: 28 July 2023
Accepted: 24 August 2023
Published: 1 October 2023

1. Introduction

Pulmonary sequestration (PS), also known as bronchopulmonary sequestration, is a rare congenital developmental malformation of the lung characterized by nonfunctional lung tissue, independent of the normal lung tissue [1,2]. PS bifurcates into intralobar (ILS) and extralobar (ELS) sequestration [3]. ILS is incorporated within the normal lung tissue and communicates with the outer bronchus through its own trachea, whereas ELS is

separated from the normal lung tissue by its own visceral pleura and presents with a lack of connection to the normal tracheobronchial tree [4].

The blood supply of nonfunctional lung tissue mainly comes from systemic circulation, especially the aorta or its branches, and most commonly from the descending thoracic aorta. It has also been reported to originate from the intercostal, phrenic, gastric, splenorenal, celiac trunk, subclavian, and innominate arteries and, more rarely, from abnormal arteries such as the coronary and pulmonary arteries [5,6]. Similarly, venous drainage varied greatly in patients with PS. In PS, the drainage of blood vessels mostly comes from the pulmonary vein (90.02%), followed by the azygos vein (4.2%), postcava (0.74%), and vena phrenica (0.21%) [6]. In most cases of ILS, the draining vein is a pulmonary vein, whereas in most cases of ELS, it is a systemic vein [7].

PS is mainly diagnosed using conventional radiology rather than invasive angiography. If such diseases are detected early, it can be an indicator of timely surgery to those requiring necessary surgical intervention, and the complications can be prevented in a timely manner which will minimize unnecessary procedures or examinations. To avoid the risk of occult or surgical bleeding, it is important to accurately identify the blood supply sources to arteries prior to surgery and eliminate the vessels during surgery [8,9]. Despite many reports on the prevalence and clinical diagnosis of PS [10–12], most have focused solely on case reports or case series. There are several retrospective studies reporting on the clinical symptoms and diagnosis of PS, either documenting PS imaging appearances in adults or pediatric patients [13–16]. Wei and Li reported the largest number of PS cases that were retrieved from the Chinese National Knowledge Infrastructure database over a period of 10 years [16]. Their analysis showed that patients with PS presented with variable clinical manifestations, with preoperative diagnosis being frequently incorrect. Of the cases that were analyzed in their study, 27% were incorrectly diagnosed before operation, of which 36% and 21% were misdiagnosed as pulmonary cyst and lung cancer, respectively. This highlights the importance of timely and correct diagnosis of PS.

In this study, we report on the computed tomography (CT) imaging features of 55 cases of PS confirmed using surgery or digital subtraction angiography (DSA) based on a multi-center experience. Our aim was to increase the diagnostic accuracy of using CT for PS and decrease the misdiagnosis rate through a comprehensive analysis of imaging characteristics. Despite reports on CT imaging findings and clinical analysis of PS available in the literature, this study serves as a useful tool to further improve the awareness of imaging spectrums and manifestations in patients with PS.

2. Materials and Methods

2.1. Patient Data Collection

We retrospectively reviewed 55 patients with PS from multiple clinical centers who underwent CT pulmonary angiography (CTPA) with PS proven via pathology or DSA. Demographic characteristics, imaging features, disease location, isolation type, and features of the supplying and draining vessels were collected for analysis. Due to the retrospective nature of the study, conducted with only reviewing de-identified images, ethics approval was waived with no requirement for patient consent.

2.2. CT Scanning and Image Interpretation

The CT scanners used were different because data were collected from multiple medical centers (64- to 256-slice scanners). While parameters for CT data acquisition varied slightly across clinical sites, the scanning protocols were as follows: tube voltage was set from 100 to 120 kV, tube current was 100–320 mA, beam collimation between 0.5 and 0.75 mm, and reconstruction slice thickness was set at 1 mm. All patients were examined using plain and dual phase contrast-enhanced CT scans. All the patients who underwent CTA examination were intravenously administered with a contrast agent (370 mg or 350 mg of iodine/mL), initiating the first phase scan when a 180 or 200 Hounsfield unit threshold was reached in the main pulmonary artery. The flow volume was 1.5 mL/kg·weight (kg),

and the flow rate was 3.5–4.0 mL/s. Pulmonary arteries were shown more brightly in this phase. Ten seconds later, the second phase was initiated, and the systemic arteries and the draining veins of PS were shown clearly in this phase.

All radiological images were available in the picture archiving and communication system from each center and analyzed using RadiAnt DICOM (Digital Imaging and Communications in Medicine) Viewer software (2020.1.1 64-bit). We generated maximum intensity projection views (MIP) to observe the blood vessels and minimum intensity projection (MinIP) to visualize the bronchus and airways. All CT images were independently reviewed by two radiologists (one with 17 years and the other with 4 years of experience in interpreting cardiothoracic CT images) who reached a consensus in case of any discrepancy.

The following details were analyzed in each case: clinical characteristics, including the types of PS—ILS or ELS; imaging features on CTPA, including the location of PS in terms of which lobes; and supplying arteries to the sequestration area and draining vessels.

2.3. Statistical Analysis

Data were analyzed using Microsoft Excel 2016 (Microsoft Corp., Redmond, WA, USA). Categorical variables were presented as percentage or frequency, while continuous variables were reported as mean and standard deviation.

3. Results

3.1. Sex Distribution and Age at Diagnosis

A total of 55 patients with PS were included in the study: 34 (61.82%) were male and 21 (38.18%) were female, with a male-to-female ratio of 1.62:1. Of the 55 cases, children aged between 3 months and 8 years accounted for 3 cases (5.45%), adolescents aged between 14 and 20 years accounted for another 3 cases (5.45%), and adults aged between 21 and 81 years accounted for 49 cases, representing the majority of cases (89.09%), with a mean age of 44 years.

3.2. Imaging Appearances of CTPA

All patients underwent chest CT examinations. Of the 55 patients, 54 (98.18%) had ILS and 1 (1.82%) had ELS (Figure 1). Pulmonary masses were found in the left lower lobe in 42 (76.36%) patients, in the right lower lobe in 12 (21.82%), and in the lower lobe of both lungs in 1 patient (1.82%). Some patients had pulmonary infection, bronchiectasis, chest pain, and lung cancer (Figure 2). In addition, some patients had other cardiovascular diseases, such as anterior descending branch-right atrial fistula and levoatriocardinal vein (LACV; Figure 3).

Forty-three (78.18%) patients had only one supplying artery and twelve (21.82%) had two or more supplying arteries. For the supplying arteries, 47 (85.45%) were derived from the descending thoracic aorta, 1 (1.82%) from the abdominal aorta, 7 (12.73%) from the celiac axis, and 1 (1.82%) from the bronchial artery. The supplying arteries were tortuous in 15 (27.27%) patients. The supplying arteries had dilated outside the lung, and the maximum diameter of the dilated artery was 13.0 mm. Similarly, in the lungs, the maximum diameter of the dilated artery was 13.0 mm.

The draining vessels were pulmonary veins in 49 patients (89.09%), umbilical vein in 1 (1.82%), venae intercostal in 1 (1.82%), pulmonary arteries in 11 (20.00%; Figure 4), and draining vessels were not shown on the plane in 2 patients (3.64%). One patient (1.82%) had significant dilatation of the drainage vessel, which was the pulmonary artery (Figure 5) (Table 1).

Figure 1. A 41-year-old female with extralobar pulmonary sequestration. (**A**) Computed tomography (CT) angiography demonstrating a sharply circumscribed cystic solid mass in the posterior mediastinum (arrow). (**B**) CT coronal images in the pulmonary window demonstrating atelectatic sequestrated lung and pleural line totally separating the normal lung parenchyma from the underlying sequestrated lung (arrow). (**C**) Contrast-enhanced CT demonstrating solid enhancement in the periphery of the posterior mediastinal mass and patchy low-density foci without enhancement in the center (arrow). A—anterior, P—posterior. (**D**) Thorax CT scan coronal image (oblique maximum intensity projection image) demonstrating blood supply to the sequestrated lung from two branches of the thoracic aorta (arrow), which are small and extended directly into the sequestrated lung.

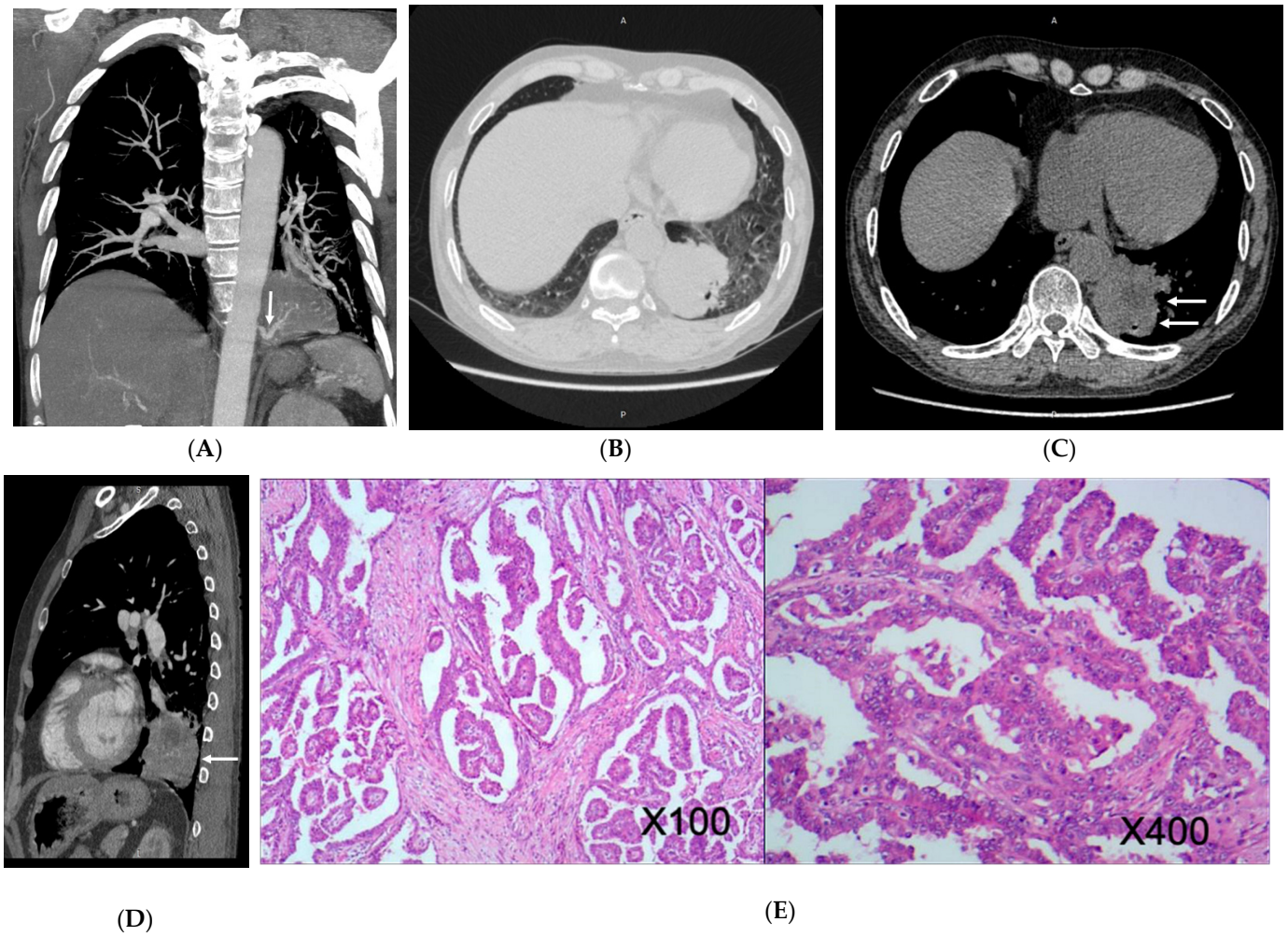

(**A**) (**B**) (**C**)

(**D**) (**E**)

Figure 2. A 68-year-old male with intralobar pulmonary sequestration. (**A**) Computed tomography angiography maximum intensity projection recombination coronal image demonstrating that the feeding artery (arrow) originates from the branch of the descending thoracic aorta, and the draining vessel is the pulmonary vein. (**B**) CT image (pulmonary windowing) demonstrating a round mass in the left lower lobe with distended margins and obstruction of the corresponding bronchus. Axial non-contrast (**C**) and sagittal contrast-enhanced (**D**) CT images demonstrating an uneven density mass with heterogeneous moderate enhancement of peripheral solid components (arrows refer to solid components of the tumor) and without any enhancement of central liquefaction necrosis. (**E**) At low magnification (×100), the tumor cells show a papillary growth pattern, and the fibrovascular axis can be seen in the stroma. Higher magnification (×400) shows cells displaying evident atypia with a high nucleoplasm ratio and a large nucleus. A—anterior, P—posterior.

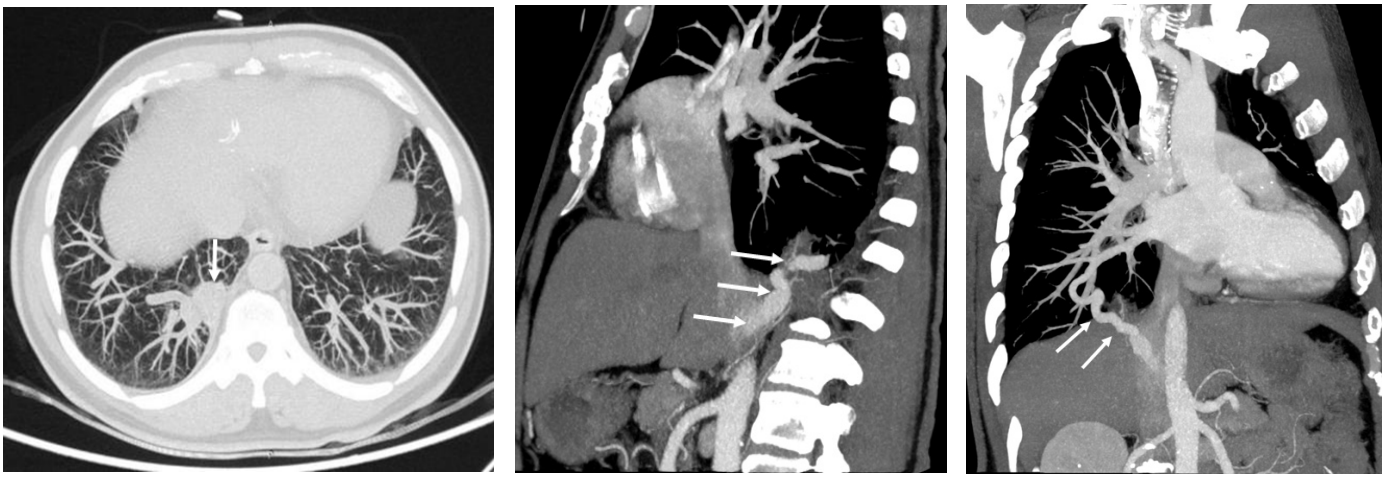

(**A**) (**B**) (**C**)

Figure 3. A 58-year-old male with intralobar pulmonary sequestration. (**A**) Intralobar pulmonary sequestration lesion in the computed tomography angiography axial image presenting as a mass (arrow) in the lower lobe of the right lung with thickening of the pulmonary vessels around it. (**B**) Oblique sagittal CTPA MIP reformatted image demonstrating that the feeding arteries arose from a branch of the abdominal aorta with a slender lumen (arrows). (**C**) Oblique coronal CTPA MIP reformatted image showing the levoatriocardinal vein (LACV) with anomalous connection between the right inferior pulmonary vein and the interior vena cava (IVC) (arrows). The normal communication between the left superior pulmonary vein (LSPV) and left atrium is not disrupted. CTPA—computed tomography pulmonary angiography, MIP—maximum intensity projection.

Table 1. Imaging appearances of chest computed tomography pulmonary angiography in patients with pulmonary sequestration (n = 55).

Imaging Appearances	Subtype	Number of Cases
Subtype of disease	ILS	54 (98.18%)
	ELS	1 (1.82%)
Location of disease	LLL	42 (76.36%)
	RLL	12 (21.82%)
	BLL	1 (1.82%)
Supplying artery	Aorta A	1 (1.82%)
	Aorta D	47 (85.45%)
	CA	7 (12.73%)
	BA	1 (1.82%)
Draining vessels	PV	49 (89.09%)
	UV	1 (1.82%)
	IV	1 (1.82%)
	PA	11 (20.00%)
	NF	2 (3.64%)

ILS, intralobar sequestration; ELS, extralobar sequestration; RLL, right lower lobe; LLL, left lower lobe; BLL, both lower lobe; Aorta A, abdominal aorta; Aorta D, descending aorta; CA, celiac axis; BA, bronchial artery; PV, pulmonary vein; UV, umbilical vein; IV, intercostal vein; PA, pulmonary artery; NF, not found.

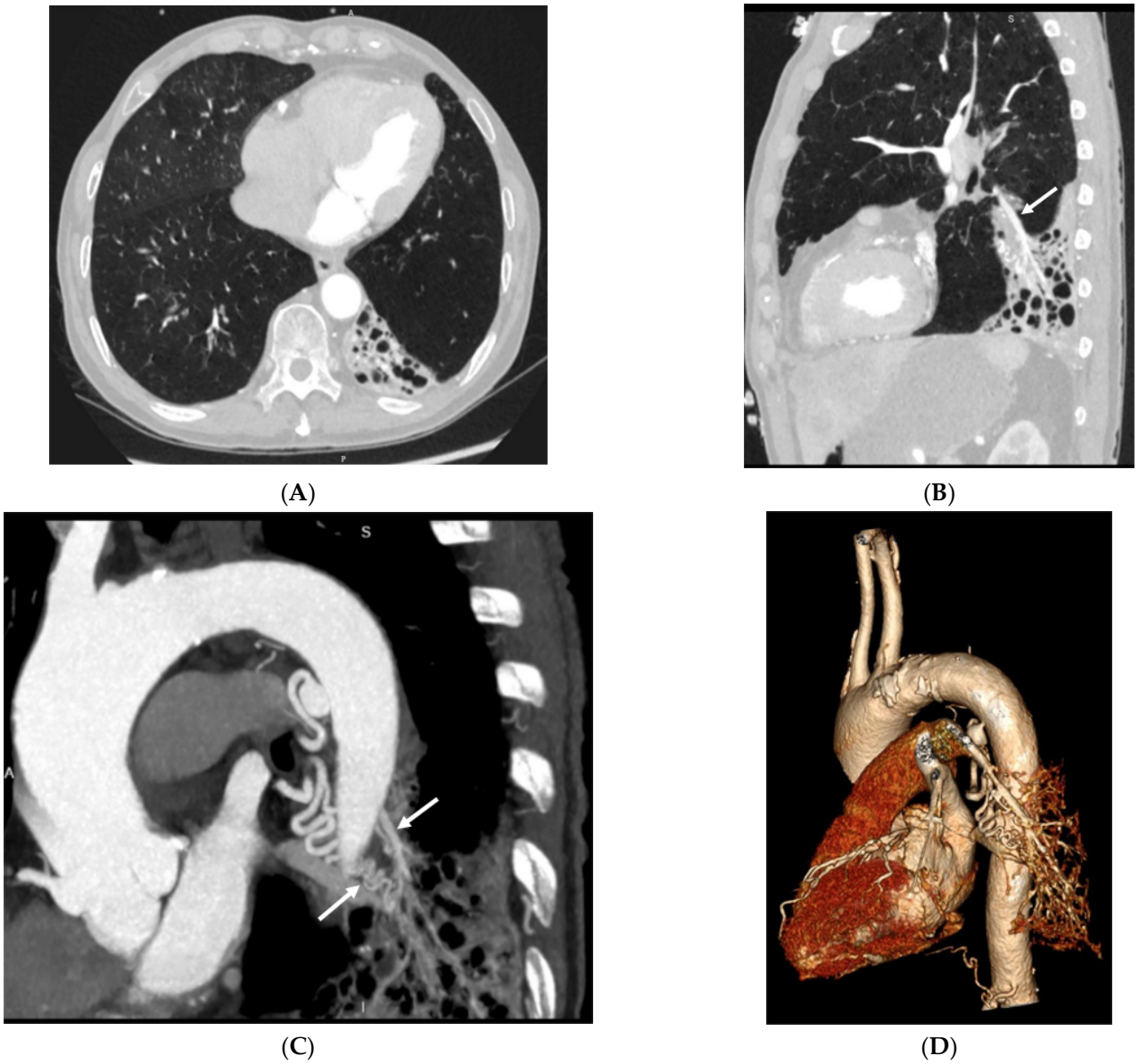

Figure 4. A 71-year-old male with intralobar pulmonary sequestration. Axial (**A**) and sagittal (**B**) computed tomography angiography demonstrating an intralobar polycystic sequestration in the lower lobe of the left lung that is cystic and heterogeneous. CTPA MIP (**C**) and volume rendering (**D**) reconstruction images of the same abnormal arterial lumen showing that both the pulmonary artery and thoracic aortic branches run to the sequestrated lung. The branch of the thoracic aorta is abnormally tortuous and has localized cystic dilation at the origin of the supplying artery. The pulmonary artery extends straight into the sequestrated lung. Arrows indicate the supplying arteries to the pulmonary sequestration. CTPA—computed tomography pulmonary angiography, MIP—maximum intensity projection. A—anterior, P—posterior, S—superior, I—inferior.

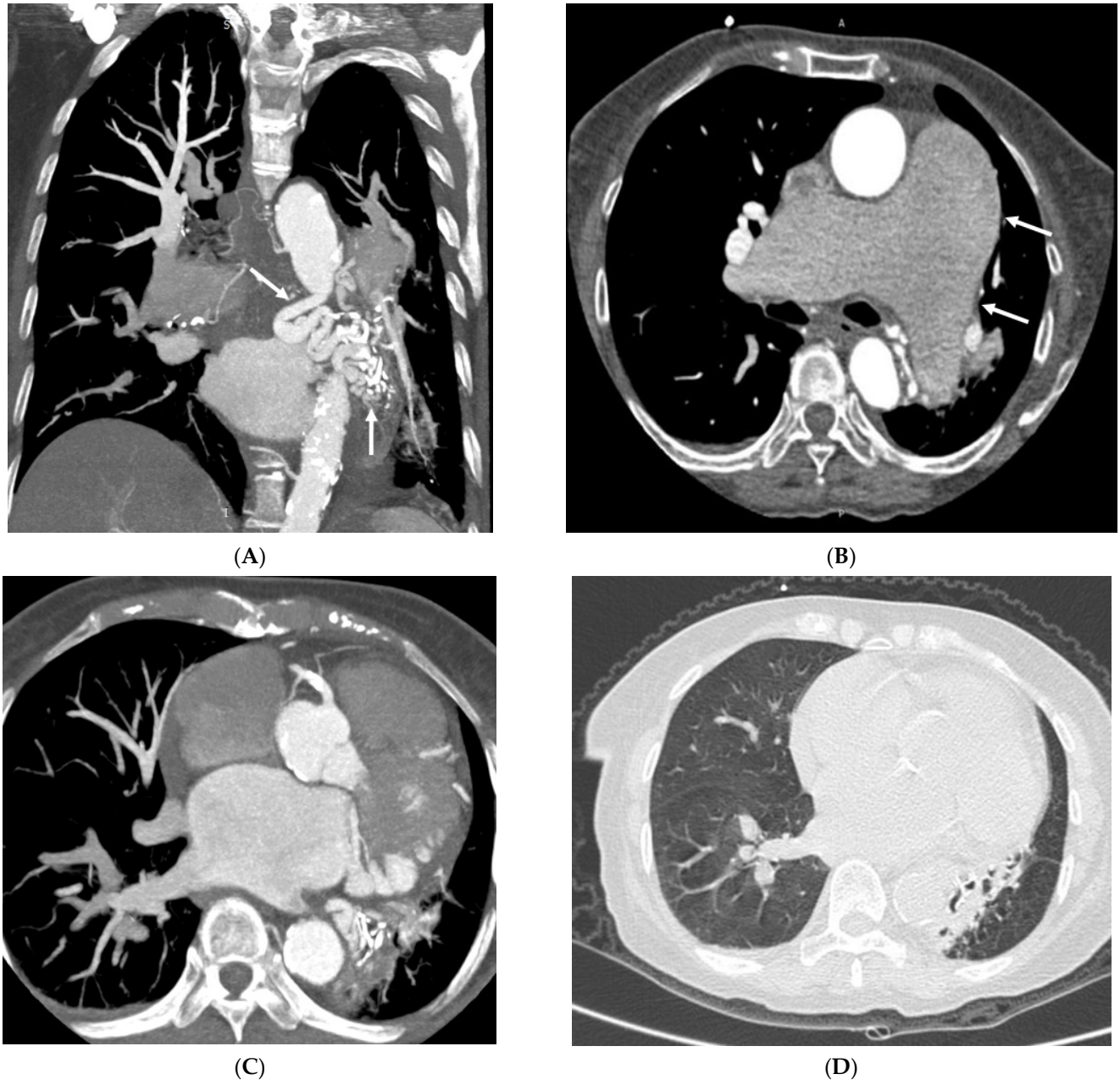

(**A**) (**B**)

(**C**) (**D**)

Figure 5. An 81-year-old female with intralobar pulmonary sequestration. (**A**) CTPA MIP reconstruction image showing that both the pulmonary artery and thoracic aortic branches extend to the sequestrated lung. The supplying arteries, the branches of the thoracic aortic, are abnormally tortuous (arrows), but the pulmonary artery extends straight into the sequestrated lung. (**B**) Axial CT scan showing that the main pulmonary trunk and pulmonary arteries to the right and left lungs are dilated (arrows). (**C**) Contrast-enhanced CT of the venous phase showing that the left inferior pulmonary vein is occluded. (**D**) Axial view of CT images (lung windowing) demonstrating a significant reduction in the volume of the left lower lung. CTPA—computed tomography pulmonary angiography, MIP—maximum intensity projection, A—anterior, P—posterior.

There were 20 (36.36%) cases of PS with bronchial atresia, 11 (20.00%) cases without bronchial atresia, and 24 (43.64%) cases where the presence of bronchial atresia could not be determined. Among these 24 cases, 2 of the third type were due to the very young age of the patients, resulting in significant respiratory artifacts on chest CT images; thus, the bronchial conditions could not be clearly observed. The other 22 patients had some degree of infection, and we did not follow-up the bronchial conditions of these patients

after anti-infection treatment. In Figure 6, a bronchial atresia in the lesion of the inferior lobe of the left lung (white arrows) is shown. Figure 7 is another example showing that the bronchus in the lower lobe of the right lung was significantly dilated, the bronchial wall was significantly thickened (black arrow), and the formation of mucus embolus in the local bronchial lumen resulted in localized bronchial occlusion.

Figure 6. A 47-year-old female with intralobar pulmonary sequestration. Sagittal minimum intensity projection (MinIP) (**A**) and coronal MinIP. (**B**) views show the bronchial atresia (white arrows) in the left inferior lower lobe.

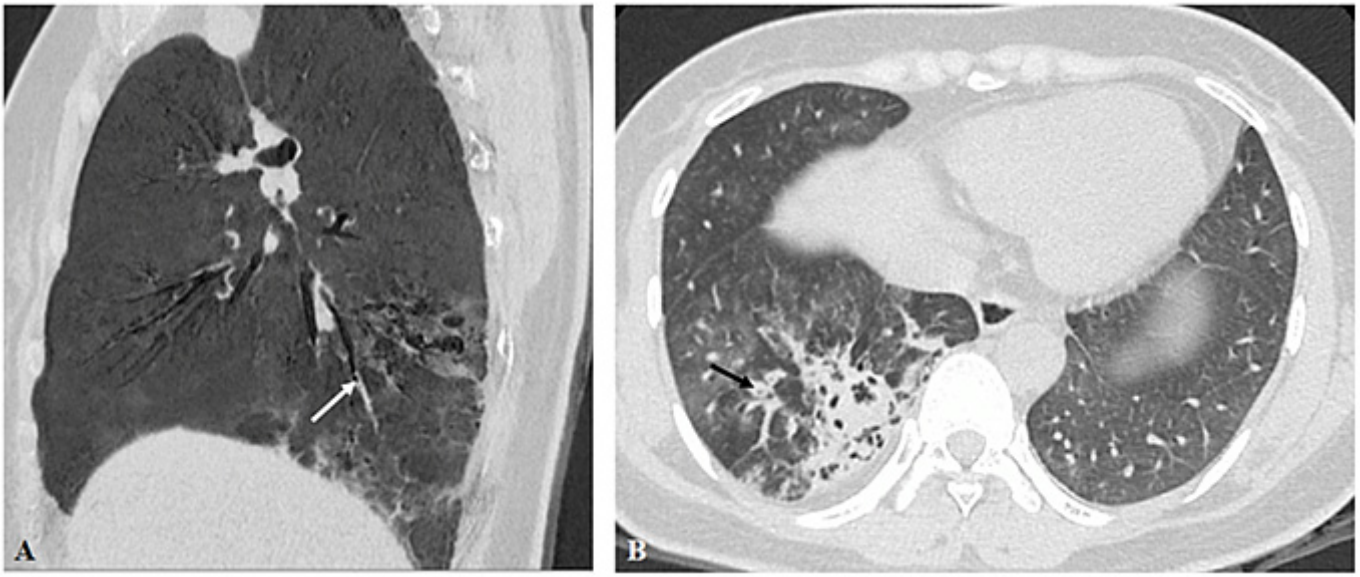

Figure 7. A 33-year-old female with intralobar pulmonary sequestration. (**A**): Sagittal minimum intensity projection view showing the occluded right lower bronchus due to mucus formation (white arrow). (**B**): Axial CT showing the dilated right lower bronchus (black arrow).

4. Discussion

This multi-center study presented CT findings of PS in both adults and pediatric patients with majority of the PS noticed in the left lower lobe than the right lower lobe. More than 80% of the supplying arteries were from the descending thoracic aorta and nearly 90% of the draining vein were from the pulmonary vein. The study findings add valuable information to the existing literature with regard to comprehensive CT analysis of patients with PS.

PS is a rare congenital developmental anomaly of unknown etiology, accounting for 0.15–6.40% of all congenital lung malformations [10], which is often found on imaging examination after symptomatic change occurs. Patients with PS can present with conditions such as recurrent pulmonary infections, chest pain, hemoptysis, and dyspnea [11]. Symptoms recur until the cause is resolved. PS is commonly associated with congenital pulmonary airway malformation (CPAM); thus, a hybrid lesion is widely used to describe the situation of PS associated with CPAM [17]. Both PS and CPAM belong to congenital cystic lung lesions and the reported cases of hybrid lesions of PS are most commonly associated with CPAM type II with aortic blood supply and pulmonary venous drainage, according to the literature [17,18]. CPAM represents an overgrowth of the terminal bronchioles leading to an abnormal connection to the tracheobronchial tree, while PS is a nonfunctional mass in the lungs with no connection to the bronchial tree. We did not find any pathological changes related to CPAM in this study after reviewing all of the CTPA findings as there was no abnormal connection of the mass to the bronchus.

ILS is the most common type of PS (75%), the most common site of which is the posterior basal segment of the left lower lobe [12]. This is also reported by other studies showing even higher prevalence of ILS, which is about 93% [13,14]. In our study, among the 55 patients, 42 had lesions located in the left lower lobe, which is in agreement with the previous literature [13–16]. ELS, which accounts for 25% of all cases of PS, is mainly located between the left lower lobe and the diaphragm adjacent to the esophagus, as well as in the pericardial region of the anterior superior mediastinum, occasionally under the diaphragm, but rarely in the middle mediastinum [13]. Previous studies have indicated that the incidence of ELS in men is approximately three- or four-fold than in women [11]. Our study included too few ELS cases to derive any comparative significance, because in our study, there was only one patient with ELS, who was a female.

In symptomatic patients or when cancer cannot be excluded, surgical resection is recommended, with mass excision being preferred for ELS and lobectomy being preferred for ILS [19]. Excessive bleeding can occur if the feeding artery is improperly ligated or destroyed during surgery; therefore, clinicians must weigh the risks of surgery and complications of PS. Consequently, it is particularly important to preoperatively identify the feeding and draining vessels. Compared with Doppler ultrasound and magnetic resonance imaging, CTPA has gradually become the primary choice for examination of PS because of the advantages of slice reconstruction, multiplanar reconstruction, 3D re-formatting, and faster scanning (reduced need for sedation and intravenous contrast media), which can also provide relevant information about the lung parenchyma, including the airway. A study by Yue et al. reported high accuracy (>95%) and sensitivity (>95%) in vessel-based evaluation of PS [20]. On our patients' CTPA images, the feeding arteries mostly arose from the descending thoracic aorta (T9–T11), and most of the draining vessels were pulmonary veins, which is consistent with the previous literature.

CTPA imaging indicated a "dual blood supply" in 11 patients, in which both the pulmonary artery and systemic circulation vessels headed into the lesion area. However, the systemic circulation vessels provide the real blood supply. The pulmonary artery does not play a role in blood supply but only plays a role in drainage, because the aorta and pulmonary artery can be visualized simultaneously in the aortic stage, whereas pulmonary artery blood flow in the direction of the lesion is stagnant in the pulmonary artery stage. Thus, we consider that the pulmonary artery of "dual blood supply" is the draining vessel but not the supplying vessel. Blood supply to the pulmonary vein will be reduced because

the pulmonary artery is a draining vessel. The pulmonary artery may become chronically dilated, and thus form pulmonary hypertension with fewer or no pulmonary veins. Over time, lung tissue atrophy on the affected side results in complete or partial occlusion of the pulmonary vein in the lesion area. Systemic circulation blood vessels always distorted abnormally in PS with "dual blood supply," which may be because the pulmonary venous return is impeded, resulting in the obstruction of pulmonary circulation and congestion of systemic circulation. Under huge pressure differences, systemic circulation blood vessels will be twisted and sometimes dilated.

The arterial support to these PS lesions are consistent with the literature as majority of the supply comes from aorta (more than 80%) [14–16]. One main difference between our findings and others is the slightly high percentage of arterial support from celiac axis which is 12.73% in our study, while this was reported to be between 8.4 and 9.3% according to studies by Long and Zhang et al. [14,15]. In contrast, only 1 out of 1808 cases was shown to have PS supplied by celiac trunk [16].

Bronchial atresia (BA) typically occurs near the central area of the lung, most commonly in the left upper lobe of the lung, and bronchial mucus plugs are often seen in the distal atresia segment. BA is a well-accepted abnormality in the majority of congenital cystic lung lesions [17,18,21]. BA refers to a lack of communication between the central airway and segmental or subsegmental bronchus. The decrease in pulmonary artery blood supply and hyperinflation in the corresponding area of BA lead to local emphysema [22,23], while PS is also local pulmonary artery hypoplasia and bronchial stenosis resulting in distal bronchiectasis and emphysema. In patients with PS, BA inevitably occurs, but there are certain differences in the typical imaging findings of BA. If BA occurs below the subsegmental level, it is difficult to distinguish whether the bronchial occlusion is caused by repeated bronchial infection in the presence of PS or due to the inherent BA. BA was found in 36% of our cases, while in nearly 44% of cases, BA could not be determined due to several reasons. Radiologists should pay attention to these findings when reviewing CTPA images to make accurate clinical diagnosis.

Patients with PS are more likely to develop other cardiovascular malformations. In one patient (Figure 3), the image showed abnormal communication between the pulmonary veins and interior vena cava (IVC), which is a type of LACV. LACV is an embryological remnant usually found on the right side, in which a malformed vessel communicates between the left atrium or pulmonary and systemic vein [24], and the pulmonary vein itself (from which the LACV arises) has normal connection with the left atrium. LACV is often associated with left-sided obstructive lesions, such as mitral atresia, aortic atresia, mitral stenosis, aortic coarctation, and hypoplastic left heart syndrome [25,26]. Under normal conditions, vascular pressure in the systemic circulation is considerably higher than that in the lungs, whereas in the systemic vein, it is considerably higher than in the pulmonary vein. However, blood flow in the LACV is directed from the pulmonary vein to the systemic venous system, which can lead to a shunt from left to right and reduce venous stasis [27]. Moreover, this abnormal connection might result in two-way flow and potential paradoxical embolism [28,29].

Malignancy in PS is exceedingly rare. Lung cancer caused by bronchopulmonary sequestration was first described by Hertzog et al. in 1963; however, the relationship between them remains unclear [30]. Malignant lesions can occur not only in the isolated lungs but also in segmental bronchi separated from the isolated lungs. In this study, in two cases of PS combined with lung cancer, malignant lesions developed in the isolated lungs. A large mass in the left lower lobe lung of patient no. 54 and in the right lower lobe lung of patient no. 55 was adjacent to the diaphragm, with an area of low density in the center. Both lesions were supplied by small branches of the descending thoracic aorta and drained by their respective pulmonary veins. If a mass is detected with an abnormal supply of blood from the systemic circulation in contrast-enhanced CT scans, it confirms the diagnosis of PS. However, surprisingly, we found cancer cells in the isolated lungs in pathology after surgery. Isolated lungs combined with malignancy usually appear as well-defined, lobulated, and

nearly round-shaped masses with swelling margins. The corresponding bronchi of the lesions were narrow and occluded. Owing to the small number of cases of PS combined with malignancy, it is important to increase the sample size and assess it repeatedly in future studies. Nonetheless, the potential for the development of malignancy combined with PS must be considered. Attention should be paid not to transect the abnormal artery of ILS during the resection of such lesions as this may cause massive bleeding.

This study has some limitations. Despite multicenter data collection, the number of PS cases was relatively small. Furthermore, we did not follow-up the patients who received treatment with regard to the clinical outcomes as our focus is on detailed analysis of the imaging features of patients with PS. We will aim to collect more cases to further advance our understanding of the PS, in particular the typical and untypical imaging appearances on CT scans so as to avoid any incorrect or missed diagnosis. Although we did not include patient treatment in this group, Zhang et al. in their recent study concluded that video-assisted thoracoscopic surgery is the treatment of choice for PS [15].

5. Future Directions of Using CTPA in PS

Use of 64 to 320-slice CT is widely prevalent in many clinical practices with acceptable spatial and temporal resolution for diagnosis of various diseases including PS. However, the latest technological developments in CT scanning with the emergence of photon-counting CT (PCT) represents a new direction in CT imaging with improved spatial resolution of 0.2 mm and a higher contrast resolution [31–35]. With a high resolution of 0.2 mm, photon-counting CT has been shown to significantly improve CT's diagnostic value in many applications including pulmonary diseases [31–36]. A recent study by Gaillandre et al. has shown the superiority of PCT over 192-slice CT by allowing for a more precise detection of CT imaging features (micronodules, linear opacities, intralobular reticulation, bronchiectasis and honeycombing) with significant lower radiation dose in patients with interstitial lung disease [36].

6. Conclusions

The clinical presentations of PS are non-specific and can be easily missed or misdiagnosed. However, CTPA can provide important clues to the diagnosis of PS by providing detailed analysis of imaging features, including supplying arteries and draining vessels. The feeding or supplying arteries mainly come from the descending aorta, while the drainage vein is the pulmonary vein. Careful analysis of CTPA images for identification of these vessels from PS plays an important role in avoiding risks or complications such as hemorrhage during surgery. With improved spatial and contrast resolution in modern CT scanners, CTPA allows for excellent visualization of lung abnormalities and airway changes which contribute to the development of optimal surgical strategies.

Author Contributions: Conceptualization, Y.L.; methodology, T.Y. and Z.W.; formal analysis, J.Q. and Q.M.; investigation, T.Y. and Z.W.; resources, T.Y., Z.W., J.Q., Q.M. and S.K.; data curation, Y.L.; writing—original draft preparation, T.Y. and Z.W.; writing—review and editing, Z.S.; visualization, J.Q. and Q.M.; supervision, Y.L.; project administration, Y.L. All authors have read and agreed to the published version of the manuscript.

Funding: This research received no external funding.

Institutional Review Board Statement: Not applicable as this is a retrospective study.

Informed Consent Statement: Patient consent was waived due to retrospective nature of the study.

Data Availability Statement: Data are not available.

Conflicts of Interest: The authors declare no conflict of interest.

References

1. Gabelloni, M.; Faggioni, L.; Accogli, S.; Aringheri, G.; Neri, E. Pulmonary sequestration: What the radiologist should know. *Clin. Imaging* **2021**, *73*, 61–72. [CrossRef] [PubMed]
2. Tsolakis, C.C.; Kollias, V.D.; Panayotopoulos, P.P. Pulmonary sequestration. Experience with eight consecutive cases. *Scand. Cardiovasc. J.* **1997**, *31*, 229–232. [CrossRef] [PubMed]
3. Yangui, F.; Charfi, M.; Abouda, M.; Charfi, M.R. Pulmonary sequestration in a healthy teenage girl. *Tunis. Med.* **2019**, *97*, 604–605.
4. Berna, P.; Lebied, E.I.D.; Assouad, J.; Foucault, C.; Danel, C.; Riquet, M. Pulmonary sequestration and aspergillosis. *Eur. J. Cardiothroac. Surg.* **2005**, *27*, 28–31. [CrossRef]
5. Salvati, F. Cardiovascular, broncho-parenchima and neoplastic anomalies related to pulmonary sequestration: A critical review. *Recenti. Prog. Med.* **2018**, *109*, 388–392.
6. Franko, J.; Bell, K.; Pezzi, C.M. Intraabdominal pulmonary sequestration. *Curr. Surg.* **2006**, *63*, 35–38. [CrossRef]
7. Ulys, A.; Samalavicius, N.; Cicenas, S.; Petraitis, T.; Trakymas, M.; Sheinin, D.; Gatijatullin, L. Extralobar pulmonary sequestration. *Int. Med. Case. Rep. J.* **2011**, *4*, 21–23.
8. Hirai, S.; Hamanaka, Y.; Mitsui, N.; Uegami, S.; Matsuura, Y. Surgical treatment of infected intralobar pulmonary sequestration: A collective review of patients older than 50 years reported in the literature. *Ann. Thorac. Cardiovasc. Surg.* **2007**, *13*, 331–334.
9. Adzic-Vukicevic, T.N.; Radovanovic, D.V.; Acimovic, B.D.; Popovic, M.P. Pulmonary sequestration mimicring lung cancer: A case report. *Vojnosanit. Pregl.* **2016**, *73*, 1060–1063. [CrossRef]
10. Tashtoush, B.; Memarpour, R.; Gonzalez, J.; Gleason, J.B.; Hadeh, A. Pulmonary sequestration: A 29 patient case series and review. *J. Clin. Diagn. Res.* **2015**, *9*, AC05-8. [CrossRef]
11. Cong, C.V.; Ly, T.T.; Minh, N.M. Intralobar pulmonary sequestration supplied by vessel from the inferior vena cava: Literature overview and case report. *Radiol. Case Rep.* **2022**, *17*, 1345–1353. [CrossRef] [PubMed]
12. Shafig, M.; Ali, A.; Dawar, U.; Setty, N. Rare cause of haemoptysis: Bronchopulmonary sequestration. *BMJ Case Rep.* **2021**, *14*, e239140. [CrossRef] [PubMed]
13. Sun, X.; Xiao, Y. Pulmonary sequestration in adult patients: A retrospective study. *Eur. J. Cardiothorac. Surg.* **2015**, *48*, 279–282. [CrossRef]
14. Long, Q.; Zha, Y.; Yang, Z. Evaluation of pulmonary sequestration with multidetector computed tomography angiography in a select cohort of patients: A retrospective study. *Clinics* **2016**, *71*, 392–398. [CrossRef] [PubMed]
15. Zhang, N.; Chen, Q.; Yu, J.; Zhang, X. Distribution, diagnosis, and treatment of pulmonary sequestration: Report of 208 cases. *J. Pediatr. Surg.* **2019**, *54*, 1286–1292. [CrossRef] [PubMed]
16. Wei, Y.; Li, F. Pulmonary sequestration: A retrospective analysis of 2625 cases in China. *Eur. J. Cardiothorac. Surg.* **2011**, *40*, e39–e42. [CrossRef]
17. Wang, D.; Wheeler, W.B. A hybrid lesion of intralobar sequestration with mixed features of CPAM type I and type II umasked following SARS-CoV-2 infection: Case report and literature review. *Int. J. Surg. Case Rep.* **2022**, *96*, 107336. [CrossRef]
18. Kunisaki, S.M. Narrative review of congenital lung lesions. *Transl. Pediatr.* **2021**, *10*, 1418–1431. [CrossRef]
19. Fukui, T.; Hakiri, S.; Yokoi, K. Extralobar pulmonary sequestration in the middle mediastinum. *Gen. Thorac. Cardiovasc. Surg.* **2017**, *65*, 481–483. [CrossRef]
20. Yue, S.W.; Guo, H.; Zhang, Y.G.; Gao, J.B.; Ma, X.X.; Ding, P.X. The clinical value of computer tomographic angiography for the diagnosis and therapeutic planning of patients with pulmonary sequestration. *Eur. J. Cardiothorac. Surg.* **2013**, *43*, 946–951. [CrossRef]
21. Naumeri, F.; Sajjad, M.N. Hybrid lesion: Extralobar sequestration with cystic adenomatoid malformation-misdiagnosed as pulmonary tuberculosis. *J. Coll. Physicians Surg. Pak.* **2018**, *28*, S204–S206. [CrossRef] [PubMed]
22. Cherian, S.V.; Kumar, A.; Ocazionez, D.; Estrada-Y-Martin, R.M.; Restrepo, C.S. Developmental lung anomalies in adults: A pictorial review. *Respir. Med.* **2019**, *155*, 86–96. [CrossRef] [PubMed]
23. Riedlinger, W.F.; Vargas, S.O.; Jennings, R.W.; Estroff, J.A.; Barnewolt, C.E.; Lillehei, C.W.; Wilson, J.M.; Colin, A.A.; Reid, L.M.; Kozakewich, H.P. Bronchial atresia is common to extralobar sequestration, intralobar sequestration, congenital cystic adenomatoid malformation, and lobar emphysema. *Pediatr. Dev. Pathol.* **2006**, *9*, 361–373. [CrossRef] [PubMed]
24. Amoretti, F.; Cerillo, A.G.; Chiappino, D. The levoatriocardinal vein. *Pediatr. Cardiol.* **2005**, *26*, 494–495. [CrossRef] [PubMed]
25. Agarwal, P.P.; Mahani, M.G.; Lu, J.C.; Dorfman, A.L. Levoatriocardinal vein and mimics: Spectrum of imaging findings. *AJR Am. J. Roentgenol.* **2015**, *205*, W162–W171. [CrossRef]
26. Saremi, F.; Ho, S.Y. Extracardiac pulmonary-systematic connection via persistent levoatriocardinal vein in adults. *Ann. Vasc. Surg.* **2016**, *34*, 269.e1–269.e7. [CrossRef] [PubMed]
27. Shet, N.; Maldjian, P. Levoatriocardinal vein: An unusual cause of right-left shunting. *J. Clin. Imaging Sci.* **2014**, *4*, 68.
28. Canan, A.; Aziz, M.U.; Abbara, S. A rate pulmonary-systemic connection: Levoatriocardinal vein. *Radiol. Cardiothorac. Imaging* **2020**, *2*, e190228. [CrossRef]
29. Karangelis, D.; Avramidis, D.; Mousiama, T.; Karamitsos, T.D.; Mitropoulos, F.; Tzifa, A. Levoatriocardinal vein: A rarely recognized cause of recurrent cardiac and cerebral thromboembolic events. *Can. J. Cardiol.* **2020**, *36*, 589.e9–589.e11. [CrossRef]
30. Hertzog, P.; Roujeau, J.; Marcou, J. Epidermoid cancer developed on a sequestration. *J. Fr. Med. Chir. Thorac.* **1963**, *17*, 33–38.

31. Koons, E.; VanMeter, P.; Rajendran, K.; Yu, L.; McCollough, C.; Leng, S. Improved quantification of coronary artery luminal stenosis in the presence of heavy calcifications using photon-counting detector CT. *Proc. SPIE Int. Soc. Opt. Eng.* **2022**, *12031*, 120311A. [CrossRef] [PubMed]
32. Zsarnoczay, E.; Fink, N.; Schoepf, U.J.; O'Doherty, J.; Allmendinger, T.; Hagenauer, J.; Wolf, E.V.; Griffith, J.P., 3rd; Maurovich-Horvat, P.; Varga-Szemes, A.; et al. Ultra-high resolution photon-counting coronary CT angiography improves coronary stenosis quantification over a wide range of heart rates-A dynamic phantom study. *Eur. J. Radiol.* **2023**, *161*, 110746. [CrossRef] [PubMed]
33. Si-Mohamed, S.A.; Boccalini, S.; Lacombe, H.; Diaw, A.; Varasteh, M.; Rodesch, P.A.; Dessouky, R.; Villien, M.; Tatard-Leitman, V.; Bochaton, T.; et al. Coronary CT angiography with photon-counting CT: First-in-human results. *Radiology* **2022**, *303*, 303–313. [CrossRef] [PubMed]
34. Hagar, M.T.; Soschynski, M.; Saffar, R.; Ran, A.; Taron, J.; Weiss, J.; Stein, T.; Faby, S.; von zur Mueblen, C.; Ruile, P.; et al. Accuracy of ultrahigh-resolution photon-counting CT for detecting coronary artery disease in a high-risk population. *Radiology* **2023**, *307*, e223305. [CrossRef] [PubMed]
35. Soschynski, M.; Hagen, F.; Baumann, S.; Hagar, M.T.; Weiss, J.; Krauss, T.; Schlett, C.L.; von zur Muhlen, C.; Nikolaou, K.; Greulich, S.; et al. High temporal resolution dual-source photon-counting CT for coronary artery disease: Initial multicenter clinical experience. *J. Clin. Med.* **2022**, *11*, 6003. [CrossRef]
36. Gaillandre, Y.; Duhamel, A.; Flohr, T.; Falvre, J.-B.; Khung, S.; Hutt, A.; Felloni, P.; Remy, J.; Remy-Jardin, M. Ultra-high resolution CT imaging of interstitial lung disease: Impact of photon-counting CT in 112 patients. *Eur. Radiol.* **2023**, *33*, 5528–5539. [CrossRef]